Influence of $pp\pi$ ions on pion absorption in H_2

S. Jonsell,[1] J. Wallenius,[2] and P. Froelich[1]
[1]*Institute for Theoretical Atomic and Molecular Physics, Harvard-Smithsonian Center for Astrophysics, 60 Garden Street, Cambridge, Massachusetts 02138*
and Department of Quantum Chemistry, Uppsala University, Box 518, S-751 20 Uppsala, Sweden
[2]*Department of Nuclear and Reactor Physics, Royal Institute of Technology, S-100 44 Stockholm, Sweden*
(Received 26 August 1998)

The existence of three-body resonances in the molecular ion $pp\pi$ has been shown by means of a variational calculation in Jacobi coordinates. The relativistic and strong-force corrections to the Coulombic binding energies and the decay widths of the resonances have been calculated. We consider two mechanisms that supply the $p\pi$ atom with large kinetic energies before the moment of pion absorption by the proton, with significant impact on the interpretation of experiments measuring the mass difference $m_{\pi^-}-m_{\pi^0}$ from pion absorption in pionic atoms. These mechanisms are (a) the formation and subsequent Coulomb decay of the metastable $pp\pi$ states and (b) pion absorption from the *molecular* $pp\pi$ state, giving, respectively, a discrete or a continuous distribution of kinetic energies of the resulting $p\pi$ atoms. [S1050-2947(99)08005-1]

PACS number(s): 36.10.−k

I. INTRODUCTION

The fate of the pions entering hydrogen is of importance for precision spectroscopy experiments, and/or experiments studying the strong-force aspects of the nuclear pion absorption by the hydrogen nuclei. The present paper addresses questions of interest for the new generation of experiments determining the strong-force shift and width of the $1s$ energy level of the $p\pi$ atom, and concentrates on problems relevant for an experiment aiming at the determination of the mass difference between negative and neutral pions, $m_{\pi^-}-m_{\pi^0}$ [1]. Knowledge of this mass difference is important in studies of the rare pion β decay through the reaction

$$\pi^{\pm}\rightarrow\pi^0+e^{\pm}+\nu \tag{1}$$

and allows tests of the standard weak interaction theory through comparisons of the predicted decay rate with experimental findings. In particular, the conserved vector current (CVC) hypothesis, predicting the same weak coupling constant G_v for pion and nucleon (pure vector) β decays, can be tested. According to this hypothesis the pion and nucleon decay rates are proportional to each other via the fifth power of the $(m_{\pi^-}-m_{\pi^0})$ mass difference [2,3].

The mass difference can be deduced from the time-of-flight studies of the neutrons produced in the capture reaction

$$\pi^-+p\rightarrow\pi^0+n \tag{2}$$

from the bound states of the pionic atoms $p\pi^-$ [4]. If the initial velocity of the pionic atoms were zero, the energy of all neutrons would be the same and could be related to the particle masses through the energy balance

$$\begin{aligned} m_{\pi^-p}&=m_{\pi^-}+m_p-E_b=E_n+E_{\pi^0}\\ &=(m_n^2+p_n^2)^{1/2}+(m_{\pi^0}^2+p_{\pi^0}^2)^{1/2}, \end{aligned} \tag{3}$$

where E_n is the neutron energy, E_{π^0} and E_n are pion and neutron (total) energies, respectively, E_b is the binding energy of the pionic atom, p_n is the momentum of the neutron, and p_{π^0} is the momentum of the neutral pion. (We have set the speed of light $c=1$.) However, the deduced mass difference is very sensitive to the initial kinetic energy of the pionic atoms, and therefore to details of the pionic cascade [5]. This aspect has become especially important in view of recent experiments which detected an excess of very energetic pionic atoms [1,6,7] and other deviations from the prevailing kinematical model. In the present paper we attempt to clarify these unexpected features of the pionic cascade with the help of our recently presented side-path theory [8–11].

The side-path theory originally relates to the muonic cascade in the mixture of deuterium and tritium during the cycle of the muon catalyzed fusion (μCF). In that cycle, the muons are captured by both deuterium and tritium forming $d\mu$ and $t\mu$, and the collisional muon transfer was previously thought to proceed one sidedly and irreversibly from deuterium to tritium. The reverse transfer was thought not possible because of the isotopic energy difference. Such a theory gave a too low population of the ground state of $d\mu(1s)$, which was inconsistent with the experiment.

We have shown that $t\mu(2s)+D_2$ collisions lead to formation of the three-body resonances $dt\mu^*$, situated in the dissociative continuum of $dt\mu$ just below the $t\mu(2s)+d$ threshold. Fast formation of these states and their following decay into the $d\mu(1s)+t$ channel can be considered as resonantly enhanced muon transfer. This opens a new mode of muon return from $t\mu$ to $d\mu$, referred to as a side path. The side-path mechanism resolved the longstanding puzzle of μCF, bringing into agreement the experimental and theoretical values of the muon cycling rate (the average time between consecutive d-t fusions) and of the population of the ground state of muonic deuterium (the so called q_{1s} fraction).

Calculations in this paper show that similar states exist below the $p\pi(nl)+p$ thresholds in pionic molecules, which similarly can be formed in $p\pi(nl)-H_2$ collisions. When the $pp\pi$ resonances decay into the $p\pi(n'l')+p$ (where n'

$<n$) channel the resulting pionic atoms will be very energetic. A competing decay channel of the $pp\pi$ molecule is the intramolecular absorption of the pion by one of the protons. We show that the vibrational motion of the protons in the molecular state will then result in an experimental signature resembling that of absorption from a $p\pi$ atom with high momentum. Thus the formation of metastable $pp\pi$ molecules opens new and previously unconsidered acceleration mechanisms for pionic atoms during the pion cascade.

In what follows we propose a new side path in the pion kinetics based on excited state chemistry of pionic atoms. We show that the rate of resonantly enhanced pion transfer via the side path is comparable to other deexcitation rates of pionic atoms. This alters the populations of low-lying states. A detailed knowledge of the populations of pionic atoms and their velocities is a prerequisite for correct interpretation of the neutron time-of-flight spectra. The objective of the present paper is to understand the influence of the side path on the mass-difference experiment outlined above.

In Sec. II we discuss how $pp\pi$ molecules can be formed and indicate their different decay channels. In Sec. III we present our calculation of the Coulombic energies of $pp\pi$ resonances. Corrections to the Coulombic energy from the strong interaction and vacuum polarization are added in Sec. IV. The Coulomb decay of the $pp\pi$ molecule, which results in a $p\pi$ atom with a discrete high kinetic energy, is studied using the method of complex scaling in Sec. V. In Sec. VI we discuss the continuous kinetic energy component from the intramolecular pion absorption. Finally we try to estimate the relevant effective rates in the pion cascade in Sec. VII.

II. FORMATION AND DECAY OF METASTABLE MOLECULAR STATES $pp\pi$

We consider the formation of a metastable hybrid molecule through the collision of a $p\pi$ atom with a H_2 molecule according to

$$(p\pi)_{nl}+(H_2)_{\nu_i K_i}\rightarrow[(pp\pi)_s pee]_{\nu K}. \tag{4}$$

Here s denotes a collection of quantum numbers, to be discussed in Sec. III below, specifying the state of the $pp\pi$ molecule, n and l are the principal and angular momentum quantum numbers of the pionic hydrogen atom, and ν_i, K_i and ν, K are vibrational and rotational quantum numbers of the initial H_2 molecule and of the metastable hybrid molecule, respectively. The resonance is formed through the Vesman mechanism [12] generalized to the *excited states* of mesic molecules [9,10]. On the scale of the H_2 molecule the $p\pi$ atom is an almost point-like neutral particle. Thus it can penetrate the electron cloud of the H_2 molecule and collide with one of its protons, forming a $pp\pi$ molecule. On the larger scale the hybrid molecule formed in this way can be regarded as an isotope of the H_2 molecule, with the $pp\pi$ molecule as one of its nuclei. The binding energy E_b of the metastable $pp\pi$ state is absorbed by a rovibrational excitation of the hydrogen molecule from the initial state $\nu_i K_i$ to the state νK of the new hybrid molecule $[(pp\pi)_s pee]$. The resonant collision energy $E_{\rm res}$ is given by

$$E_{\rm res}=\Delta E_{\rm rovib}-E_b, \tag{5}$$

where $\Delta E_{\rm rovib}$ is the increase in rovibrational energy. Thus the Vesman mechanism requires the existence of metastable states of the $pp\pi$ molecule with a binding energy less than the dissociation energy of H_2 ($\simeq 4.5$ eV). In the following section we will show that such states indeed do exist.

The metastable state can decay through a number of different channels. There is decay back to the initial channel,

$$[(pp\pi)_s pee]_{\nu K}\rightarrow(p\pi)_{nl_f}+(H_2)_{\nu_f K_f}, \tag{6}$$

Auger decay,

$$[(pp\pi)_s pee]_{\nu K}\rightarrow[(pp\pi)_{s_f} pe]_{\nu_f K_f}+e^-, \tag{7}$$

radiative decay,

$$[(pp\pi)_s pee]_{\nu K}\rightarrow[(pp\pi)_{s_f} pee]_{\nu K}+\gamma, \tag{8}$$

Coulomb decay,

$$(pp\pi)_s\rightarrow(p\pi)_{n_f l_f}+p, \tag{9}$$

and nuclear absorption,

$$(pp\pi)_s\rightarrow p+n+\pi^0. \tag{10}$$

When the metastable state decays through Coulomb decay, Eq. (9), the $p\pi$ atom in the final state will gain the kinetic energy

$$T_{p\pi}=\frac{\mu_{p\pi}}{m_e}\left(\frac{1}{n_f^2}-\frac{1}{n_i^2}-E_b\right)\Big/\left(1+\frac{m_p+m_\pi}{m_p}\right)\ \text{Ry}, \tag{11}$$

where 1 Ry $=13.6057$ eV, m_e is the mass of the electron, and $\mu_{p\pi}=121.497$ MeV/c^2 is the pion-proton reduced mass.

The Coulomb decay can take place either directly or after an intermediate Auger decay, Eq. (7), or radiative decay, Eq. (8). The latter intermediate processes will stabilize the molecule against backscattering, Eq. (6), but not against nuclear absorption. Possible acceleration of pionic atoms through nuclear absorption from a molecular state will be discussed in Sec. VI. The most important task is therefore to establish the existence of three-body resonances in $pp\pi$ which would be accessible to the Vesman formation mechanism, and to estimate whether the Coulomb decay or the intramolecular absorption of these resonances can compete with other decay processes.

III. COULOMBIC ENERGY LEVELS OF METASTABLE $pp\pi$

The energy eigenvalues of $pp\pi$ were obtained variationally by use of the coupled rearrangement channel method devised by Kamimura [13]. This method uses Jacobian coordinates in *both* rearrangement channels a,b shown in Fig. 1. The Hamiltonian included all nonrelativistic Coulomb interactions without any simplifying approximations. This Hamiltonian is invariant under rotations of the entire molecule, inversion of *all* spatial coordinates $\mathcal{I}$($\mathcal{I}\mathbf{r}_\alpha=-\mathbf{r}_\alpha$, and $\mathcal{I}\mathbf{R}_\alpha=-\mathbf{R}_\alpha$, $\alpha=a,b$), and inversion of the internuclear co-

FIG. 1. The Jacobian coordinate systems used. The origin of R_i is at the center of mass of the two particles connected by r_i.

ordinate only (i.e., spatial permutation of the two protons) $\mathcal{I}_n$ ($\mathcal{I}_n\mathbf{r}_b=-\mathbf{r}_b$, and $\mathcal{I}_n\mathbf{R}_b=\mathbf{R}_b$). The symmetry of the wave function can thus be characterized by the corresponding quantum numbers $J=0,1,\ldots,\ M_J=-J,\ldots,J,\ p=\pm1$ and $q=\pm1$. Here J and M_J are the usual rotational quantum numbers and the quantum numbers p and q are defined through

$$\mathcal{I}\Phi^{pq}_{JM_J}=p(-1)^J\Phi^{pq}_{JM_J}, \tag{12}$$

$$\mathcal{I}_n\Phi^{pq}_{JM_J}=q(-1)^J\Phi^{pq}_{JM_J}. \tag{13}$$

Different states of the same symmetry are designated by the quantum number n of the nearest higher atomic threshold, and a vibrational quantum number v. Thus the molecular state is fully specified by $s=\{n,v,J,M_j,p,q\}$. Obviously the pion inversion operator (defined by $\mathcal{I}_\pi\mathbf{r}_b=\mathbf{r}_b$, $\mathcal{I}_\pi\mathbf{R}_b=-\mathbf{R}_b$) is $\mathcal{I}_\pi=\mathcal{I}\mathcal{I}_n$. Thus the states can be classified as *gerade/ungerade* symmetry according to whether $pq=\pm1$.

The wave function Φ^{pq}_{JM}, is expanded in terms of Gaussian basis functions spanned over the two rearrangement channels $\alpha=a,b$.

$$\Phi^{pq}_{JM_J}=\sum_\alpha\sum_{l,L}\sum_{i=1}^{i_{\max}}\sum_{I=1}^{I_{\max}}\frac{c_{\alpha ilIL}}{\sqrt{2}}[1+q(-1)^J\mathcal{I}_n]g_{\alpha ilIL}, \tag{14}$$

$$g_{\alpha ilIL}=r_\alpha^l R_\alpha^L e^{-(r_\alpha/r_{\alpha i})^2}e^{-(R_\alpha/R_{\alpha I})^2}[Y_l(\hat{\mathbf{r}}_\alpha)\otimes Y_L(\hat{\mathbf{R}}_\alpha)]_{JM_J}, \tag{15}$$

where for each rearrangement channel l is the angular momentum of the two-body subsystem connected by $\mathbf{r}_\alpha$, and L is the angular momentum of the third particle with respect to this subsystem. Of course l and L are not conserved separately, but vectorially add up to the conserved total angular momentum J. The nonlinear variational parameters $r_{\alpha i}$ and $R_{\alpha I}$ are chosen as

$$r_{\alpha i}=r_{\alpha 1}\left(\frac{r_{\alpha n}}{r_{\alpha 1}}\right)^{(i-1)/(i_{\max}-1)},$$
$$R_{\alpha I}=R_{\alpha 1}\left(\frac{R_{\alpha N}}{R_{\alpha 1}}\right)^{(I-1)/(I_{\max}-1)}. \tag{16}$$

The geometrical progression allows for an accurate description of both short and long range behavior.

Since the two protons are identical the third possible rearrangement channel (see Fig. 1) was not needed after the program had been modified to include the exchange contribution. Thus the number of Gaussians necessary to obtain a given accuracy has been halved, and consequently execution times and memory requirements were reduced by almost 75%. The sizes of the largest basis sets used for the different symmetries are shown in Table I.

TABLE I. Sizes of the largest basis sets used for the different symmetries. N is the number of Gaussians, $\mathcal{N}$ the number of configurations $\{\alpha,l,L\}$ summed over in Eq. (14), and $l_{\max}$ is the highest angular momentum included.

J	q	p	N	$\mathcal{N}$	$l_{\max}$
0	1	1	2751	7	4
0	−1	1	2063	7	4
1	1	1	4564	9	3
1	−1	1	4280	9	3
1	1	−1	2545	6	4
1	−1	−1	1680	5	4

The resonances are embedded in the scattering continuum of free $p\pi(n=1,2)$, so the Rayleigh-Ritz procedure will not be applicable. Instead we apply the stabilization technique [8], where one introduces a real scaling parameter α through the transformation

$$r\to r\alpha,\quad T\to T/\alpha^2,\quad V\to V/\alpha,$$

where T and V are the kinetic and potential energy matrix elements, respectively. Varying α one obtains a stabilization graph as shown in Fig. 2 from where the resonant energies can be deduced. The stabilization technique based on real scaling delivers the resonance position on the energy scale. To obtain the concomitant lifetimes a complex scaling parameter must be used; such a calculation is presented in Sec. V.

We present our calculated energy eigenvalues in eV relative to the thresholds for dissociation to a pionic hydrogen atom and a proton, where the atomic energies are given by

$$E_n=-\frac{\mu_{p\pi}}{m_e}\frac{1}{n^2}\ \text{Ry},\quad n=1,2,\ldots. \tag{17}$$

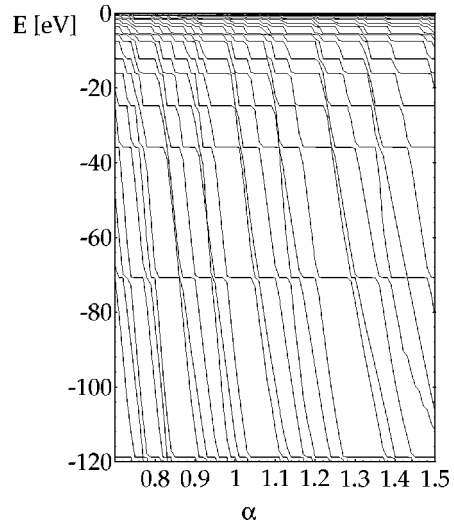

FIG. 2. Stabilization graph showing metastable states of the $pp\pi$ molecule below the $n=3$ threshold with symmetry $J=0$, $p=q=1$.

TABLE II. Binding energies E_b of $pp\pi$ resonances under the $n=2$ threshold. For each (p,q) symmetry the three columns contain the binding energy from the three-body calculation, the binding energy in the Born-Oppenheimer approximation, and the Born-Oppenheimer designation of the state.

$J=0$	v		$p=q=1$			$p=1,\ q=-1$	
	0	236.17	232.33	$3d\sigma_g$	21.06	20.31	$4f\sigma_u$
	1	100.15	98.85	$3d\sigma_g$	5.77	5.50	$4f\sigma_u$
	2	26.62	26.55	$3d\sigma_g$	1.57	1.48	$4f\sigma_u$
	3	6.76	6.59	$3d\sigma_g$			
	4	1.82	1.74	$3d\sigma_g$			
$J=1$	v		$p=q=1$			$p=1,\ q=-1$	
	0	220.37	214.44	$3d\sigma_g$	18.67	17.59	$4f\sigma_u$
	1	89.63	86.72	$3d\sigma_g$	13.18	5.90	$2p\pi_u$
	2	21.84	21.00	$3d\sigma_g$	4.76	4.45	$4f\sigma_u$
	3	5.30	4.95	$3d\sigma_g$	1.23	1.12	$4f\sigma_u$
	4	1.35	1.23	$3d\sigma_g$			
$J=1$	v		$p=-1,\ q=1$				
	0	13.11	5.90	$2p\pi_u$			

We have calculated energy eigenvalues for both bound and metastable states up to the $n=3$ threshold for rotational symmetries $J=0,\ 1$ and $p,\ q=\pm 1$. Our results reveal three truly bound states with $J\leqslant 1$, all with the proton inversion symmetry $q=1$. For inversion symmetry $p=1$ we found one bound state for each J, with binding energies relative to the $n=1$ atomic threshold -294.86 eV for $J=0$, and -80.23 eV for $J=1$. For $p=-1$ we found one bound state with $J=1$ and binding energy -13.11 eV relative to the $n=2$ atomic threshold.

The stabilized eigenvalues for $n=2,\ 3$ and $J=0,\ 1$ are shown in Tables II and III. The first column shows the eigenvalues obtained with Coulomb interaction only. For comparison we also show the energies obtained using the Born-Oppenheimer approximation. The potential curves were calculated using the method described in [14], while the rovibrational problem was solved using the program LEVEL 6.0 by LeRoy [15].

When the Born-Oppenheimer approximation is applied there are several ways in which the Hamiltonian can be separated into electronic, rovibrational, and neglected terms [16]. We used the reduced proton-pion mass in the kinetic term of the electronic Hamiltonian since with this choice one obtains the correct atomic threshold energies. Notice that this choice invalidates the proof that the Born-Oppenheimer energy is a lower bound for the correct energy as given in [17]. For $\Lambda \neq 0$ states (where Λ is the electronic angular momentum along the internuclear axis) the centrifugal barrier may be introduced in several ways. We have used the standard prescription $[J(J+1)-\Lambda^2]/R^2$ (where J still is the *total* angular momentum of the molecule). This choice was found to give the most exact energies for the $5g\pi$ and $4f\pi$ states. For the $2p\pi$ state, however, the Born-Oppenheimer energy using this prescription is far off, -5.90 eV compared to the exact value -13.18 eV. For this case a much better Born-Oppenheimer energy -13.48 eV was obtained by removing the centrifugal barrier altogether.

The errors of the Born-Oppenheimer energies are smaller for $pp\pi$ than for asymmetric exotic molecules like $dt\mu$ since for symmetric molecules the energy of the dissociation limit is correct in the Born-Oppenheimer approximation.

Let us now discuss the consequences of the the angular momenta l and L of the two sub-systems p-π and p-p for p symmetry. Within the framework of the Born-Oppenheimer approximation L is the rotational quantum number of the nuclei, which in this approximation is a conserved quantum number, and l is the angular momentum of the pion, whose projection m along the internuclear axis is conserved. On the other hand, in a nonadiabatic treatment such as ours only the *total* angular momentum J is conserved. Thus the angular part of the wave function is a sum over combinations of l,L of the type $[Y_l(\hat{\mathbf{r}}_\alpha)\otimes Y_L(\hat{\mathbf{R}}_\alpha)]_{JM_J}$ [cf. Eq. (15)]. From the definition of $\mathcal{I}$ and Eq. (12) one then sees that $p=(-1)^{J+l+L}$, since according to the rules for adding angular momenta $|L-l|\leqslant J\leqslant L+l$ one sees that for $J=0$ only $p=1$ is possible, while for $J>0$ both parities $p=\pm 1$ are possible. Within the Born-Oppenheimer approximation the $p=\pm 1$ states are degenerate. This degeneracy is the same as for the two possible projections along the internuclear axis of the pion angular momentum, $m=\pm|m|$, when $|m|>0$. When the full Hamiltonian is considered m is no longer a conserved quantum number, and thus the degeneracy is broken. In terms of nonadiabatic couplings between Born-Oppenheimer states the full Hamiltonian includes a coupling between the σ and π states. But for $p=-1$ no σ state exists, and thus the σ-π coupling is absent. By comparing the energies of the $p=-1$ states with the energies of the corresponding $p=+1$ states in Table III one can then deduce that the contribution from the σ-π coupling to the total nonadiabatic energy shift is on the order of 0.1 eV.

Notice that it is not possible for a $p=-1$ state to dissociate to an s-state atom. Therefore the first dissociation threshold for $p=-1$ states is the $n=2$, and consequently any $p=-1$ state with energy less than this threshold energy is a truly bound state embedded in a continuum of a different

TABLE III. Binding energies E_b of $pp\pi$ resonances under the $n=3$ threshold. For each (p,q) symmetry the three columns contain the binding energy from the three-body calculation, the binding energy in the Born-Oppenheimer approximation, and the Born-Oppenheimer designation of the state.

$J=0$	v		$p=q=1$			$p=1,\ q=-1$	
	0	118.78	118.28	$5g\sigma_g$	24.73	23.93	$6h\sigma_u$
	1	70.78	70.77	$5g\sigma_g$	12.17	11.71	$6h\sigma_u$
	2	35.91	36.19	$5g\sigma_g$	5.81	5.53	$6h\sigma_u$
	3	16.11	16.11	$5g\sigma_g$	2.76	2.60	$6h\sigma_u$
	4	7.51	7.38	$5g\sigma_g$	1.31	1.22	$6h\sigma_u$
	5	5.48	4.65	$4d\sigma_g$	0.62	0.57	$6h\sigma_u$
	6	3.53	3.43	$5g\sigma_g$			
	7	1.68	1.60	$5g\sigma_g$			
	8	0.80	0.75	$5g\sigma_g$			
	9	0.38	0.35	$5g\sigma_g$			
$J=1$	v		$p=q=1$			$p=1,\ q=-1$	
	0	116.37	115.58	$5g\sigma_g$	72.46	72.15	$4f\pi_u$
	1	68.81	68.56	$5g\sigma_g$	30.78	31.12	$4f\pi_u$
	2	34.42	34.54	$5g\sigma_g$	23.84	23.05	$6h\sigma_u$
	3	15.22	15.15	$5g\sigma_g$	11.58	11.13	$6h\sigma_u$
	4	10.02	10.24	$5g\pi_g$	8.80	9.28	$4f\pi_u$
	5	7.01	6.86	$5g\sigma_g$	5.47	5.19	$6h\sigma_u$
	6	3.30	3.16	$5g\sigma_g$	2.74	2.94	$4f\pi_u$
	7	3.24	3.40	$5g\pi_g$	2.56	2.41	$6h\sigma_u$
	8	1.98	1.24	$4d\sigma_g$	1.15	1.12	$6h\sigma_u$
	9	1.50	1.46	$5g\sigma_g$	0.81	0.97	$4f\pi_u$
	10	1.01	1.14	$5g\pi_g$	0.52	0.52	$6h\sigma_u$
	11	0.67	0.68	$5g\sigma_g$			
	12	0.30	0.31	$5g\sigma_g$			
	13	0.24	0.38	$5g\pi_g$			
$J=1$	v		$p=-1,\ q=1$			$p=-1,\ q=-1$	
	0	72.51	72.15	$4f\pi_u$	10.10	10.24	$5g\pi_g$
	1	30.87	31.12	$4f\pi_u$	3.30	3.40	$5g\pi_g$
	2	8.96	9.28	$4f\pi_u$	1.09	1.14	$5g\pi_g$
	3	2.82	2.94	$4f\pi_u$	0.36	0.38	$5g\pi_g$
	4	0.92	0.97	$4f\pi_u$			

symmetry. Similar ''anomalous parity'' states have previously been calculated for muonic molecules [18].

IV. CORRECTIONS

The eigenvalues calculated with the purely Coulombic Hamiltonian have been corrected for vacuum polarization and the strong interaction between the pion and the protons.

In the calculation of the energy shifts and widths due to the strong nuclear force we assumed a contact interaction between pointlike particles. Using the coordinates in Fig. 1 the strong interaction can be represented by a pseudopotential [19]

$$V_{\mathrm{SI}}=C(1+\mathcal{I}_n)\,\delta(\mathbf{r}_a), \tag{18}$$

where the operator $\mathcal{I}_n$ ensures that the interaction with the second proton is included. First order perturbation theory with respect to the complex pseudopotential V_{SI} then gives the energy shift ΔE_{SI}, and the width Γ_{SI} [20],

$$\Delta E_{\mathrm{SI}}=2\ \mathrm{Re}\{C\}\int |\Phi^{pq}_{JM}(\mathbf{r}_a=\mathbf{0},\mathbf{R}_a)|^2 d\mathbf{R}_a\,, \tag{19}$$

$$\Gamma_{\mathrm{SI}}/2=-2\ \mathrm{Im}\{C\}\int |\Phi^{pq}_{JM}(\mathbf{r}_a=\mathbf{0},\mathbf{R}_a)|^2 d\mathbf{R}_a\,. \tag{20}$$

We have determined the constant $C=-(1.8+0.12i)a_0^3$ eV (where a_0 is the pionic Bohr radius) from the experimental value of the strong interaction shift for the pionic hydrogen atom in its $1s$ state $\Delta E_{1s}=-7.1$ eV, and $\Gamma_{1s}=0.97$ eV [21], respectively.

The vacuum polarization was calculated using the method described in [22].

Energy corrections for the states under the $n=2$ and $n=3$ are shown in Tables IV and V, respectively. The energy shifts of the $1s$, $2s$, and $3s$ *atomic* states due to the strong interaction are -7.1 eV, -0.89 eV, -0.26 eV and due to vacuum polarization -3.24 eV, -0.37 eV, -0.11 eV, respectively. For p and d states the strong interaction shifts

TABLE IV. Corrections to the Coulombic binding energies E_b of $pp\pi$ resonances under the $n=2$ threshold. The first and second columns show the increase in binding energy due to vacuum polarization ΔE_{VP} and to the strong interaction ΔE_{SI}, respectively. The third column is the corrected binding energy relative to the shifted atomic $2s$ threshold for $p=1$, and relative to the $2p$ threshold for $p=-1$.

		ΔE_{VP}	ΔE_{SI}	E_b	ΔE_{VP}	ΔE_{SI}	E_b
$J=0$	v		$p=q=1$			$p=1,\ q=-1$	
	0	0.29	0.64	235.84	0.20	0.44	20.45
	1	0.23	0.51	99.63	0.21	0.44	5.16
	2	0.21	0.45	26.02	0.21	0.45	0.97
	3	0.21	0.45	6.16			
	4	0.21	0.45	1.22			
$J=1$	v		$p=q=1$			$p=1,\ q=-1$	
	0	0.28	0.61	220.00	0.19	0.42	18.03
	1	0.22	0.49	89.09	0.04	0.02	11.99
	2	0.20	0.44	21.23	0.20	0.44	4.15
	3	0.20	0.44	4.69	0.21	0.45	0.63
	4	0.21	0.45	0.75			
$J=1$	v		$p=-1,\ q=1$				
	0	0.03	0.00	13.10			

vanish. There is, however, still a small vacuum polarization shift for the p states, -0.04 eV for $2p$ and -0.01 eV for $3p$.

The combined (vacuum polarization plus strong interaction) energy shifts of the *molecular* states classified as π states in the Born-Oppenheimer approximation are very small. This is to be expected since these states have small pion densities at the protons. The combined energy corrections to the *bound* states under the $n=1$ threshold due to the strong interaction and vacuum polarization are -11.53 eV for $J=0$, and -10.20 eV for $J=1$.

The rate for pion absorption Γ_{abs} is obtained from Eq. (20). For σ states close to the nth threshold we have found $\Gamma_{\mathrm{abs}}=\Gamma_{1s}/n^4=1.47\times10^{15}/n^4\ \mathrm{s}^{-1}$ to be a good approximation. This can be understood since states close to the threshold can be viewed as a $p\pi_{nl}$ atom perturbed by the second proton. Through the Stark effect the electric field from the second proton will mix all n possible values of the quantum number l statistically. Thus the probability for $l=0$ is $1/n$, which, multiplied by the atomic s-state pion density at the proton $|\psi_{ns}(0)|^2=|\psi_{1s}(0)|^2/n^3$, gives the estimate cited above.

Any molecular resonant state with inversion symmetry $p=1$ [cf. Eq. (12)] which gets shifted just above an ns threshold will decay very rapidly because it couples strongly to the continuum in which it is embedded. Since the molecular states normally are shifted less than the atomic s state the result will be that the molecular resonant states with an (uncorrected) binding energy very close to the threshold will disappear. In Tables IV and V we present the binding energy relative to the *shifted* atomic threshold.

The states with inversion symmetry $p=-1$ form an exception. As discussed above they *cannot* dissociate to an atom in an s state. Also, since they do not couple to σ states, the pion density at the protons will vanish completely. Consequently, according to Eqs. (19) and (20) there is no energy shift due to the strong interaction, and pion absorption by the protons will not occur. The energy shift caused by vacuum polarization for these $(p=-1)$ states is small, about -0.006 eV for the states under the $n=3$ threshold, and -0.03 eV under the $n=2$ threshold.

V. COULOMBIC LIFETIMES

In order to calculate the Coulombic lifetimes we employed the method of complex scaling [23]. The complex dilatation operator is defined as

$$U(\theta)f(\mathbf{r})=e^{3\theta/2}f(e^{\theta}\mathbf{r}). \tag{21}$$

The complex dilated Hamiltonian is then

$$H(\theta)=U(\theta)HU^{-1}(\theta)=e^{-2\theta}T+e^{-\theta}V. \tag{22}$$

The stationary solutions of the complex dilated eigenvalue problem correspond to the complex energies of the resonances. To assure θ independence of resonances (guaranteed by the exact theory) the eigenvalues of the concomitant matrix eigenvalue problem are stabilized with respect to the condition $\partial E/\partial\theta=0$.

The dilatation operation leaves the overlap matrix $\mathbf{S}$ unchanged. One can therefore reduce the generalized eigenvalue problem $\mathbf{H}(\theta)c^{\theta}=E^{\theta}\mathbf{S}c^{\theta}$ to a standard eigenvalue problem by a single Cholesky decomposition [24] of $\mathbf{S}=\mathbf{L}\mathbf{L}^{\mathrm{T}}$, where $\mathbf{L}$ is lower triangular, for all θ. The resulting eigenvalue problem

$$\mathbf{L}^{-1}\mathbf{H}(\theta)(\mathbf{L}^{\mathrm{T}})^{-1}c^{\theta}=E^{\theta}c^{\theta} \tag{23}$$

is complex symmetric. This symmetry can be utilized by reducing $\mathbf{L}^{-1}\mathbf{H}(\theta)(\mathbf{L}^{\mathrm{T}})^{-1}$ to a tridiagonal matrix using the Lanczos method [24,25]. We have also used reduction to a

TABLE V. Corrections to the Coulombic binding energies E_b of $pp\pi$ resonances under the $n=3$ threshold. The first and second columns show the increase in binding energy due to vacuum polarization ΔE_{VP} and to the strong interaction ΔE_{SI}, respectively. The third column is the corrected binding energy relative to the shifted atomic threshold. The $p=-1$ states are omitted from the table since their strong interaction shift is 0, and their vacuum polarization shift is small, typically -0.006 eV.

		ΔE_{VP}	ΔE_{SI}	E_b	ΔE_{VP}	ΔE_{SI}	E_b
$J=0$	v		$p=q=1$			$p=1,\ q=-1$	
	0	0.06	0.13	118.60	0.04	0.09	24.49
	1	0.05	0.11	70.57	0.04	0.09	11.93
	2	0.05	0.09	35.68	0.04	0.09	5.57
	3	0.04	0.09	15.87	0.04	0.09	2.52
	4	0.04	0.09	7.27	0.04	0.09	1.07
	5	0.03	0.08	5.22	0.05	0.09	0.38
	6	0.04	0.09	3.29			
	7	0.04	0.09	1.44			
	8	0.04	0.09	0.56			
	9	0.05	0.10	0.17			
$J=1$	v		$p=q=1$			$p=1,\ q=-1$	
	0	0.06	0.13	116.19	0.01	0.00	72.10
	1	0.05	0.11	68.60	0.01	0.00	30.42
	2	0.04	0.09	34.19	0.04	0.09	23.60
	3	0.04	0.09	14.98	0.04	0.09	11.34
	4	0.01	0.00	9.66	0.01	0.00	8.44
	5	0.04	0.09	6.77	0.04	0.09	5.23
	6	0.04	0.09	3.06	0.01	0.00	2.38
	7	0.01	0.01	2.89	0.04	0.09	2.32
	8	0.03	0.08	1.72	0.05	0.09	0.92
	9	0.04	0.09	1.26	0.01	0.01	0.46
	10	0.01	0.01	0.66	0.05	0.09	0.29
	11	0.05	0.09	0.44			
	12	0.05	0.10	0.08			

Hessenberg matrix by the Arnoldi method [24]. We found that the latter method, although more time consuming, was numerically more stable.

The complex calculation is more demanding computationally than the real stabilization technique presented in Sec. III. Therefore it limits the length of the expansion (14). The positions of resonances obtained by the real stabilization technique are used as the starting point for the complex stabilization based on $\partial E/\partial\theta=0$. It should be kept in mind that it is the complex procedure which gives the correct resonance positions, and the real stabilization technique gives only approximate values. On the other hand, the smaller basis sets necessitated by the complex procedure imply slower convergence.

We present in Table VI the complex energies for the number of resonances for which reasonably good convergence was obtained. An exception is the $n=3$, $v=4$ state, which in the Born-Oppenheimer approximation is the ground state of the $4d\sigma_g$ potential. At most 3904 Gaussians were used. The convergence of the results as a function of basis-set size is shown in Table VII for a few representative resonances. Examples of paths in the complex plane for the state $J=v=0$, $p=q=1$ under the $n=2$ threshold are given in Fig. 3.

For states closer to the threshold the imaginary part of the energy becomes progressively smaller, and therefore no reliable widths could be obtained. The same is true for states with $q=-1$ symmetry.

The above mentioned properties of the Coulomb width can be understood through a qualitative argument. Since the average interproton distance of the molecular states is large, the pion density will be concentrated close to one of the protons in a state resembling a Stark mixed state of the $p\pi$ atom. If the perturbation from the weakly bound second proton is small this state is orthogonal to all atomic states with different principal quantum number n. (The $4d\sigma_g$ state again will have a shorter binding distance and thus be more nonadiabatic than $5g\sigma_g$ states of comparable energy.) Thus the probability for Coulomb decay will decrease with decreasing binding energy close to threshold. In fact the most likely path for the Coulomb decay is the transfer of the pion from one proton to the other [26], i.e., since the protons are identical, through the exchange mechanism. The probability for Coulomb decay depends on the magnitude of the wave function for small interproton distances. For $q=-1$ states the pion density is zero at the midpoint between the protons. Thus the pion density of a $q=-1$ state is generally more concentrated at the protons, while for a $q=+1$ state there is some accumulation of pion density between the protons. Thus the prob-

TABLE VI. Results from complex scaling for states of symmetry $J=0$, $p=q=1$ under the $n=2,3$ thresholds. The columns show the corresponding atomic threshold, the vibrational quantum number, the real and imaginary parts of the energy, and the Coulomb width $\Gamma_{\mathrm{Coul}}=2\,\mathrm{Im}\{E\}/\hbar$. The corrections due to vacuum polarization and strong interaction are not included in this table.

n	v	Re$\{E\}$ (eV)	Im$\{E\}$ [meV]	Γ $(10^{12}\ \mathrm{s}^{-1})$
2	0	−236.17	−1.3	4.1
2	1	−100.15	−1.9	5.7
2	2	−26.62	−0.9	2.7
2	3	−6.76	−0.2	0.6
3	0	−118.78	−6	18
3	1	−70.78	−8	24
3	2	−35.91	−10	30
3	3	−16.11	−5	15
3	5	−5.48	−8	24

ability for *transfer* of the pion from one proton to the other, as in the Coulomb decay, is less likely for a $q=-1$ state.

VI. INTRAMOLECULAR ABSORPTION OF THE PION

The pion in a $pp\pi$ state may of course be absorbed by one of the protons before the three-body state has decayed through any of the other channels. Here we investigate the effects from such an intramolecular absorption on a neutron time-of-flight spectrum.

In this context it is important to understand exactly how a kinetic energy in the initial channel may cause a line broadening of the neutron time-of-flight spectrum. Let us first consider the case where pion absorption occurs from a pionic atom with binding energy E_n and no kinetic energy. For the sake of clarity we treat the problem nonrelativistically and set $\hbar=c=1$. The relativistic treatment is given in [27].

The nonrelativistic energy balance is, from Eq. (3),

$$m_{\pi^-}+m_p-E_n=m_n+\frac{k_n^2}{2m_n}+m_{\pi^0}+\frac{k_{\pi^0}^2}{2m_{\pi^0}}. \qquad (24)$$

From momentum conservation $k_n=k_{\pi^0}$. The binding energy E_n varies with the order of 100 eV between different atomic thresholds. In principle one should have a separate peak in the neutron time of flight spectrum for every different initial state n.

Let us investigate the sensitivity of the time of flight with regard to the change of the initial $p\pi$ binding energy. The relative variation of neutron momentum relates to a variation of the binding energy $\Delta E\simeq 100$ eV as

$$\left|\frac{\Delta k_n}{k_n}\right|=\frac{\mu_{n\pi}}{k_n}\left|\frac{\Delta E}{k_n}\right|\simeq 1.5\times 10^{-5}, \qquad (25)$$

where $\mu_{n\pi}$ is the n-π^0 reduced mass and $k_n=28$ MeV, the corresponding change in the neutron time of flight at the distance l is $|\Delta t|\simeq(2\times 10^{-3}\ \mathrm{ns/m})\,l$. Since this difference is small compared to experimental resolution we may replace E_n in Eq. (24) by its average value $\overline{E_n}$. We define $Q=m_{\pi^-}-m_{\pi^0}+m_p-m_n-\overline{E_n}=3.3$ MeV.

Now, let us see what happens if the pionic atom has an initial kinetic energy $T_{p\pi}\simeq 10$ eV. The energy balance gives

TABLE VII. Convergence of the real and complex parts of the resonance energy (in eV) as a function of the number of Gaussians in the basis set.

N	$n=2,\ v=0$	$n=2,\ v=3$	$n=3,\ v=0$	$n=3,\ v=3$	$n=3,\ v=5$
2500	−236.17303	−6.76326	−118.7782	−15.966	−5.48030
	−0.00133i	−0.00011i	−0.0091i	−0.015i	−0.0059i
3000	−236.17312	−6.76339	−118.779	−16.116	−5.48179
	−0.00137i	−0.00023i	−0.0075i	−0.028i	−0.0089i
3300	−236.17310	−6.76338	−118.7801	−16.1078	−5.4815
	−0.00136i	−0.000185i	−0.0064i	−0.0075i	−0.0081i
3500	−236.17314	−6.76339	−118.7805	−16.1058	−5.4820
	−0.00133i	−0.000175i	−0.0070i	−0.0054i	−0.0084i
3700	−236.17312	−6.76341	−118.7807	−16.108	−5.4819
	−0.001367i	−0.000181i	−0.0063i	−0.0047i	−0.0085i
3784	−236.17312	−6.76340	−118.7811	−16.1065	−5.4820
	−0.001385i	−0.000174i	−0.0062i	−0.0049i	−0.0080i
3904	−236.17312	−6.76341	−118.7814	−16.1081	−5.4821
	−0.001340i	−0.000186i	−0.0057i	−0.0031i	−0.0083i

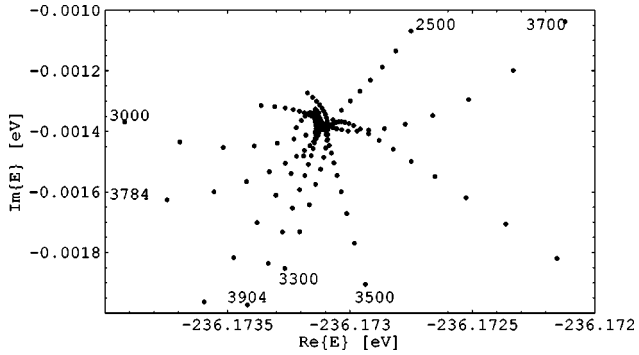

FIG. 3. Scaling paths in the complex plane using different basis sets for the state $n=2$, $J=0$, $v=0$, $p=q=1$. The numbers in the graph indicate the number of Gaussians used to calculate the different scaling paths. The markers show steps of 0.01 rad in the complex scaling parameter θ. The resonance is located at $E=-236.173-0.0013i$ eV.

$$Q+T_{p\pi}=\frac{k_n^2}{2m_n}+\frac{k_{\pi^0}^2}{2m_{\pi^0}}. \tag{26}$$

We have just seen that the addition (or subtraction) of an energy <100 eV in the initial channel does not considerably change the neutron time of flight. By the same argument we can neglect $T_{p\pi}$ on the left of Eq. (26). However, since we are now adding a *translational* kinetic energy rather than an *internal binding energy* there will also be an effect from the conservation of momentum.

The neutron time of flight changes because the center of mass of the p-π^- system (and consequently the n-π^0 system) is moving with a momentum $\mathbf{k}$ (in the laboratory system). To see the effect of this we write down the energy balance, neglecting $T_{p\pi}$ but including the additional momentum $\mathbf{k}$ in the momentum balance

$$Q=\frac{k_n^2}{2m_n}+\frac{k_{\pi^0}^2}{2m_{\pi^0}}, \tag{27}$$

$$\mathbf{k}_n+\mathbf{k}_{\pi^0}=\mathbf{k}. \tag{28}$$

Inserting Eq. (28) in Eq. (27) and neglecting another term of order $T_{p\pi}$ one has

$$Q=\frac{k_n^2}{2\mu_{n\pi}}-\frac{k_n k\cos\theta}{m_{\pi^0}}, \tag{29}$$

where θ is the angle between $\mathbf{k}_n$ and $\mathbf{k}$. Thus one has

$$\frac{\Delta k_n}{k_n}=\frac{\mu_{n\pi}}{m_{\pi^0}}\cos\theta\frac{\Delta k}{k_n}=4.6\times10^{-3}\cos\theta, \tag{30}$$

where $\Delta k=2(m_p+m_{\pi^-})T_{p\pi}\simeq0.15$ MeV. The change in neutron time of flight is then $\Delta t=(0.5\ \text{ns/m})l\cos\theta$). Thus the broadening of the peak in the neutron time-of-flight spectrum is symmetric and of the order of nanoseconds, which is two orders of magnitude larger than the change due to the indetermination of the initial binding energy.

Turning now to pion absorption from a $pp\pi$ state the energy balance reads

$$Q-E_b=\frac{k_n^2}{2m_n}+\frac{k_{\pi^0}^2}{2m_{\pi^0}}+\frac{k_p^2}{2m_p}, \tag{31}$$

where $E_b\simeq10$ eV is the additional molecular binding energy, and k_p is the final momentum of the ''spectator'' proton, i.e., the proton that does not take part in the nuclear reaction. None of the energy released by the pion absorption will be transferred to the spectator proton because the final-state interaction ceases to exist due to the neutrality of the decay fragments. Thus k_p will be determined by the initial motion of the proton, i.e., by the molecular vibrations. Within the framework of the Born-Oppenheimer approximation, the maximum k_p can be determined from the depth of the potential well. For a given proton separation the total kinetic energy of the molecular vibration can then be estimated from the distance between the potential curve of the electronic state and the energy of the vibrational state. This kinetic energy is shared between the two protons. Under the $n=3$ the depth of the deepest potential well is about 120 eV, giving a maximum kinetic energy of the spectator proton of about 60 eV. The kinetic energies of the neutron and the pion are about three orders of magnitude larger than that of the proton in the final state.

Once again we neglect all energies less than 100 eV in Eq. (31) and write down the momentum balance (assuming the molecule is initially at rest)

$$Q=\frac{k_n^2}{2m_n}+\frac{k_{\pi^0}^2}{2m_{\pi^0}}, \tag{32}$$

$$\mathbf{0}=\mathbf{k}_n+\mathbf{k}_{\pi^0}+\mathbf{k}_p. \tag{33}$$

Equations (32) and (33) are identical to Eqs. (27) and (28) with $\mathbf{k}=-\mathbf{k}_p$. Thus, pion absorption from a $pp\pi$ state where the spectator proton has the final momentum k_p gives the same broadening of the neutron time-of-flight spectrum as pion absorption from a $p\pi$ atom with initial momentum k_p. The corresponding kinetic energy that a free atom would have to have in order to give the same broadening, i.e., the ''apparent'' kinetic energy of the intra-molecular pion absorption with final proton momentum k_p, is then $T_{p\pi}=k_p^2/2(m_p+m_{\pi^-})$.

In order to calculate the distribution of apparent kinetic energies $T_{p\pi}$ from an intra-molecular pion absorption we give below a rigorous derivation, i.e., beyond the Born-Oppenheimer approximation, of the corresponding k_p distribution.

The strong interaction Hamiltonian can be represented in terms of creation and annihilation operators for particle type i at position $\mathbf{x}$, $a_i(\mathbf{x})$ and $a_i^\dagger(\mathbf{x})$, as

$$H_{\mathrm{SI}}=C'\int a_n^\dagger(\mathbf{x})a_p(\mathbf{x})a_{\pi^0}^\dagger(\mathbf{x})a_{\pi^-}(\mathbf{x})d\mathbf{x}(+\mathrm{H.c.}), \tag{34}$$

where $\mathbf{x}$ is the position where the absorption occurs.

Since two out of the three particles in the final state are neutral the final wave function is simply a product of plane waves of the proton, neutron, and neutral pion,

$$\Psi_f(\mathbf{r}_p,\mathbf{r}_n,\mathbf{r}_{\pi^0})=\frac{1}{(2\pi)^{9/2}}e^{i\mathbf{k}_p\cdot\mathbf{r}_p}e^{i\mathbf{k}_n\cdot\mathbf{r}_n}e^{i\mathbf{k}_{\pi^0}\cdot\mathbf{r}_{\pi^0}}, \quad (35)$$

where $\mathbf{k}_a$ and $\mathbf{r}_a$ are the wave vectors and positions in the laboratory system of the respective particles.

Using the form Eq. (34) for the strong interaction, and the initial and final wave functions, Eqs. (14) and (35), the transition rate for the intramolecular absorption is

$$w_{fi}=\frac{4\pi C'}{(2\pi)^9\hbar}\left|\int\int e^{-i(\mathbf{k}_n+\mathbf{k}_{\pi^0})\cdot\mathbf{x}}e^{-i\mathbf{k}_p\cdot\mathbf{r}_p}\Phi_{JM}^{pq}\times(0,\mathbf{r}_p-\mathbf{x})d\mathbf{r}_p d\mathbf{x}\right|^2\delta(E_i-E_f), \quad (36)$$

where we have multiplied the rate by a factor 2 to account for the possibility of absorption occurring at both protons. It is worth noticing that, notwithstanding the constant C', Eq. (36) expresses a rigorous transition rate due to the fact that the exact final wave function is available for neutral particles. We now make the change of variables

$$\mathbf{R}=\mathbf{r}_p-\mathbf{x}, \quad (37)$$

$$\mathbf{R}_{\rm cm}=\frac{1}{m_{\pi^0}+m_p+m_n}[m_p\mathbf{r}_p+(m_n+m_{\pi^0})\mathbf{x}], \quad (38)$$

and integrate over $\mathbf{R}_{\rm cm}$, to obtain

$$w_{fi}=\frac{4\pi C'}{(2\pi)^3\hbar}\left|\int e^{-i\mathbf{k}_p\cdot\mathbf{R}}\Phi_{JM}^{pq}(\mathbf{0},\mathbf{R})d\mathbf{R}\right|^2\times\delta(E_i-E_f)\,\delta(\mathbf{k}_n+\mathbf{k}_{\pi^0}+\mathbf{k}_p). \quad (39)$$

The (laboratory frame) velocity of the neutron in the final state is about $0.03c$ [1]. It is thus adequate to use nonrelativistic kinematics. The dependence on k_p in the final-state energy E_f can be neglected since $k_p \ll k_n, k_{\pi^0}$. Integrating Eq. (39) first over $\mathbf{k}_{\pi^0}$, which eliminates the δ function of the momenta, we can then use the relation

$$\frac{\partial k_n}{\partial E_f}=\frac{\hbar^2 k_n}{2\mu_{n\pi}} \quad (40)$$

to eliminate the δ function of energy by integrating over $\mathbf{k}_n$. The transition rate to the momentum space element $d\mathbf{k}_p$ is then

$$w_{fi}=\frac{4C'\mu_{n\pi}k_n}{\pi\hbar^3}\left|\int e^{-i\mathbf{k}_p\cdot\mathbf{R}}\Phi_{JM}^{pq}(\mathbf{0},\mathbf{R})d\mathbf{R}\right|^2 d\mathbf{k}_p, \quad (41)$$

where k_n now is a constant determined by the energy balance. Writing $\Phi_{JM}^{pq}(\mathbf{0},\mathbf{R})=\phi(R)Y_{JM}(\hat{\mathbf{R}})$, and using the relation

$$e^{i\mathbf{k}_p\cdot\mathbf{R}}=4\pi\sum_{l=0}^{\infty}\sum_{m=-l}^{l}i^l j_l(k_pR)Y_{lm}^*(\hat{\mathbf{k}}_p)Y_{lm}(\hat{\mathbf{R}}), \quad (42)$$

Eq. (41) is simplified to

$$w_{fi}=(4\pi)^2\frac{4C'\mu_{n\pi}k_n}{\pi\hbar^3}\left|\int j_J(k_pR)\phi(R)R^2dR\right|^2 k_p^2 dk_p, \quad (43)$$

which is the momentum-differential transition rate. In order to normalize it we will divide Eq. (43) by the total rate, which is most conveniently obtained by integrating Eq. (41) over $d\mathbf{k}_p$. We get

$$w_{fi}(\text{total})=(2\pi)^3\frac{4C'\mu_{n\pi}k_n}{\pi\hbar^3}\int|\phi(R)R^2|^2dR. \quad (44)$$

This result corresponds to Eq. (20) above. The normalized probability that after a given absorption from a $pp\pi$ state the spectator proton will have momentum between $\hbar k_p$ and $\hbar(k_p+dk_p)$ is then

$$P(k_p)dk_p=\frac{2}{\pi}\left|\int j_J(k_pR)\phi(R)R^2dR\right|^2 k_p^2dk_p\Big/\int|\phi(R)|^2R^2dR. \quad (45)$$

The apparent kinetic energy $T_{p\pi}$ from the intramolecular absorption will form a continuous distribution. The acceleration of pionic atoms through Coulombic deexcitations will give peaks at some discrete energies. For the resonance mediated Coulomb decay of a $pp\pi$ state Eq. (9) these energies are given by Eq. (11), while for the direct Coulombic deexcitation process

$$(p\pi)_{n_i}+p\rightarrow(p\pi)_{n_f}+p \quad (46)$$

Eq. (11) can be used inserting $E_b=0$. In Ref. [7] the experimental data were fitted to four such high energy peaks corresponding to the $n_i\rightarrow n_f$ transitions $6\rightarrow5$, $5\rightarrow4$, $4\rightarrow3$, and $3\rightarrow2$ (the component from $2\rightarrow1$ is too small to be seen in experiments). All peaks except the one with highest kinetic energy, theoretically 209 eV, coming from the $3\rightarrow2$ transition, showed fitted energies significantly *below* the theoretical value [7]. One reason for this could be that the Coulombic deexcitation occurs via a molecular state as described above, and thus according to Eq. (11) the gain of kinetic energy has to be reduced by the molecular binding energy. For the states in the Vesman region this reduction is only a couple of eV, but if there is an intermediate Auger decay the binding energy has to be at least 15 eV (the ionization energy of H_2), reducing the energy gain by more than 7 eV. This argument does, however, require that the formation of $pp\pi$ molecules competes favorably with the direct Coulombic deexcitation Eq. (46) also for more highly excited pionic atoms.

Another reason could be that in addition to the discrete

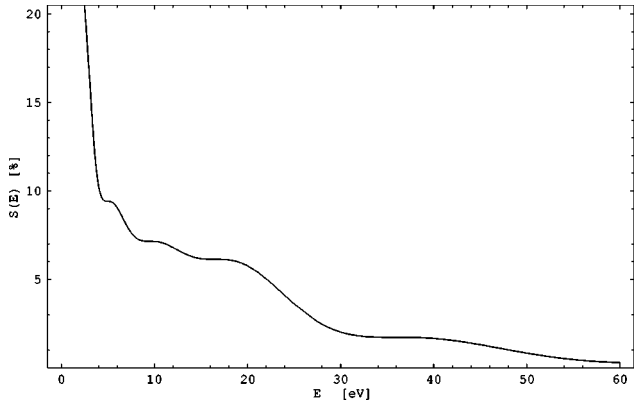

FIG. 4. Nuclear absorption from the three-body resonance $n=3, J=0, p=q=1, v=6$. $S(E)$ shows the probability that the apparent kinetic energy of a pionic atom $T_{p\pi}$ is larger than E.

peaks there is a continuous component originating from the presence of intramolecular absorption. It is then sufficient that a significant amount of $pp\pi$ molecules are formed from one of the excited states of the $p\pi$ atom. For instance, a continuous distribution originating from the intramolecular absorption from $pp\pi$ states formed from $p\pi$ atoms with $n=3$ would extend into the energy region where discrete peaks from (either direct or resonance mediated) Coulomb decay of more highly excited atoms are located, shifting these peaks. It would, however, not affect the fitted energy of the discrete $n_i=3\rightarrow n_f=2$ peak at 209 eV since the continuous distribution does not extend to such high kinetic energies. Whether or not a continuous distribution from intramolecular absorption does significantly affect the experimental results of course depends on how large it is compared to the discrete peaks.

An example of how nuclear absorption from the three-body state $n=3, J=0, p=q=1, v=6$ can mimic the effect of accelerated pionic atoms is shown in Fig. 4. On the y axis the quantity $S(E)=\int_E^\infty P(T_{p\pi})dT_{p\pi}$, i.e., the probability that the apparent kinetic energy $T_{p\pi}$ is larger than E is shown (in percent). As one would expect from a simple Born-Oppenheimer picture the acceleration is very small in most cases. We do, however, see that a tail extends to higher energies, one has $T_{p\pi}>1$ eV for 36% of all absorptions, and $T_{p\pi}>10$ eV for 7% of all absorptions. Thus we predict that in addition to the sharp peaks there should also be a continuous component in the spectrum. At $T_{p\pi}\simeq 60$ eV this component vanishes completely, which is consistent with depth of the potential curve, which is roughly 120 eV, and corresponds to approximately 50%-50% partitioning of the kinetic energy between the two protons in the initial channel. Figure 4 shows the contribution from one resonance only; as the contributions from several resonances are added the distribution will be smoother.

VII. DISCUSSION

Our calculations indicate that several $pp\pi$ states exist within the energy region accessible to the formation mechanism according to Eq. (4). To determine whether this mechanism really is relevant in the pionic cascade one has to calculate the partial formation rates leading to all the different decay processes, Eqs. (6),(7),(8),(9),(10).

All rates mentioned above can be used to construct the cross section for the resonant formation and decay of the $pp\pi$ molecule, by means of the Breit-Wigner formula

$$\sigma_r=\frac{\pi}{k^2}\frac{\Gamma_{\rm ent}\Gamma_r}{(E-E_{\rm res})^2+(\Gamma_{\rm ent}+\Gamma_{\rm Aug}+\Gamma_{\rm Coul}+\Gamma_{\rm abs})^2/4}, \tag{47}$$

where $r=\{\text{ent, Aug, Coul, abs}\}$, and Γ_r is the partial width of the corresponding decay channel. From Eq. (47) we obtain the partial rates for formation of a $pp\pi$ state and its decay through channel r as

$$\lambda_r=\rho v\sigma_r, \tag{48}$$

where ρ is the density (which here will be assumed to be liquid hydrogen density), and v is the relative velocity between the $p\pi$ atom and the H_2 molecule in the initial channel. The Breit-Wigner formula does not take into account the interferences between different resonances. In a more careful analysis one is required to diagonalize the coupling matrices between all possible degenerate and nondegenerate states of the hybrid and $pp\pi$ molecules and the final and initial channels. Here we are, however, only making a first estimate of the formation rates.

The widths for formation and back decay, Eqs. (4),(6), and for Auger decay, Eq. (7), of muonic resonances under the $n=2$ threshold were investigated in [10]. Using these results as an estimate for pionic molecules, and assuming that similar values are valid under the $n=3$ threshold, we obtain $\Gamma_{\rm ent}\simeq 10^{13}$–$10^{14}$ s^{-1} and $\Gamma_{\rm Aug}\simeq 10^{12}$–$10^{13}$ s^{-1}.

Our complex scaling calculations for the Coulomb width were not able to give converged widths for vibrational states close to the threshold. Extrapolating the width dependence of low-lying vibrational states, we can, however, deduce that close to the $n=2$ threshold the widths are $<10^{11}$ s^{-1}, and close to the $n=3$ threshold $<10^{12}$ s^{-1}. Thus the Coulomb decay channel will be less important than Auger decay for the states that can be formed by the Vesman mechanism. It is, however, possible that perturbations from the surroundings will increase the Coulomb width. The resonances close to the thresholds are states with a quite large separation between the protons. Thus they are not small on the scale of the H_2 molecule. To improve the calculation it is therefore advisable to include the effects from the surrounding H_2 system.

For more deeply bound resonant states the Coulomb decay channel becomes more important, while the perturbations from the surroundings are less important. As has already been discussed (and presented in Table VI) the Coulomb widths reach 5×10^{12} s^{-1} for $n=2$, and 3×10^{13} s^{-1} for $n=3$.

For the pion absorption width we use the results from Sec. IV, i.e., for vibrational states in the Vesman region $\Gamma_{\rm abs}=9.2\times 10^{13}$ s^{-1} under the $n=2$ threshold and $\Gamma_{\rm abs}=1.8\times 10^{13}$ s^{-1} under the $n=3$ threshold. The rate for radiative decays [cf. Eq. (8)] is typically orders of magnitude smaller so it can be neglected. The estimated partial widths are summarized in Table VIII.

TABLE VIII. Estimates of the partial widths for the various channels in s^{-1}. Γ_{ent} is the width for entering the resonance and for back decay, Γ_{abs} the width for nuclear absorption, Γ_{Aug} the Auger width, Γ_{Coul} the Coulomb width, and Γ_{rad} the radiative width.

Width (s^{-1})	$n=2,\ J=0,\ p=q=0,\ v=4$	$n=3,\ J=0,\ p=q=0,\ v=7$
Γ_{ent}	10^{13}–10^{14}	10^{13}–10^{14}
Γ_{abs}	10^{14}	2×10^{13}
Γ_{Aug}	10^{12}–10^{13}	10^{12}–10^{13}
Γ_{Coul}	$\simeq10^{10}$–5×10^{12}	$\simeq10^{11}$–3×10^{13}
Γ_{rad}	$\simeq10^{11}$	$\simeq2\times10^{10}$

In Fig. 5 we illustrate how estimates of the formation rate λ_{Aug} (for states close to threshold) depend on the collision energy. In these estimates we have used the cross section given by Eq. (47) with $\Gamma_{ent}=10^{13}\ s^{-1}$ (assumed to be approximately constant), $\Gamma_{Aug}=2\times10^{12}\ s^{-1}$, $\Gamma_{Coul}=3\times10^{11}\ s^{-1}$. In the first frame we illustrate a σ state where $\Gamma_{abs}=1.8\times10^{13}\ s^{-1}$. The second frame illustrates a π state where $\Gamma_{abs}\simeq0$. By inspecting formula (47) one sees that the partial rates for nuclear absorption and Coulomb decay are $\lambda_{abs}=\lambda_{Aug}\Gamma_{abs}/\Gamma_{Aug}\simeq9\lambda_{Aug}$ (for the σ state) and $\lambda_{Coul}=\lambda_{Aug}\Gamma_{Coul}/\Gamma_{Aug}\simeq0.15\lambda_{Aug}$. The rate is sensitive both to the widths of the competing channels in the denominator of Eq. (47) and to the resonance energy E_{res}. The precision in E_{res}, and thus through Eq. (5) in E_b and ΔE_{rovib}, necessary for an accurate calculation of the partial rates is about 0.01 eV.

Note that each curve in Fig. 5 represents the contribution to the total rate from *one* metastable $pp\pi$ state only. From Table V one sees that under the $n=3$ threshold there are seven states of $J=0$ symmetry and 12 states of $J=1$ symmetry within the energy region ($E_b<4.5$ eV) accessible to formation by the Vesman mechanism. Each of these will contribute with a different partial rate, and at a different resonant energy E_{res}. The resonant energy is obtained by matching the binding energy of the $pp\pi$ state with the energy of the most suitable rovibrational excitation of the hybrid molecule (5). The separation between the vibrational levels of the hybrid molecule is about 0.4 eV, which consequently should be the maximum value of E_{res}. As the contributions from all resonances are included the overall rate should therefore both increase at maximum and should be relatively large over a wider range (0–$E_{res}^{max}\simeq0.4$ eV) of collisional energies.

After the Auger process the pion will be bound with a binding energy of at least the ionization energy of H_2, 15.5 eV. Thus the final state after Auger decay lies outside the Vesman region, and therefore it cannot decay back into the initial channel. The two dominant decay processes from this state will be Coulomb decay and intramolecular pion absorption. According to Table VI the Coulombic rate from the final state after Auger decay is for the states of symmetry $J=0,\ p=q=1$ under the $n=2$ threshold at least $\Gamma_{Coul}=2.7\times10^{12}\ s^{-1}$, which is much less than the rate for nuclear absorption, $\Gamma_{abs}=10^{14}\ s^{-1}$.

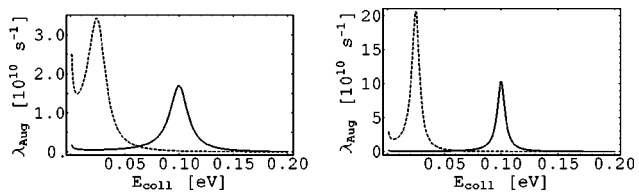

FIG. 5. An estimate of λ_{Aug} (for the formation of $pp\pi$ followed by its Auger decay) using Eq. (47) and the widths in the text. The left frame is for a σ state and the right frame for a π state (no pion absorption). In both frames the solid line is $E_{res}=0.1$ eV and the dashed line $E_{res}=0.025$ eV. Liquid hydrogen density has been assumed.

Under the $n=3$ threshold our calculations predict a state ($J=0,\ v=3,\ p=q=1$) with binding energy that barely exceeds the minimum energy released during the Auger transition. This state could therefore be populated very effectively through Auger decay from a very weakly bound resonant state. The Coulomb decay width for this state is $\Gamma_{Coul}=1.5\times10^{13}\ s^{-1}$, which is of the same order as the rate for nuclear absorption $\Gamma_{abs}=2\times10^{13}\ s^{-1}$. Other more deeply bound resonant states with somewhat larger Coulomb widths also exist. Thus we expect a sizable fraction of the Auger decays under the $n_i=3$ threshold to finally give an acceleration of the pionic atom by the energy characteristic for the direct Coulomb decay less the molecular binding energy Eq. (11). For the Auger decays that are not followed by an acceleration through the Coulomb decay the intramolecular pion absorption gives a high energy component of $T_{p\pi}$ even larger than for the state shown in Fig. 4 (because the wave function is confined to smaller R values) but it will extend to a somewhat lower maximum energy (because of the larger binding energy of the state).

The $pp\pi^*$ side path (characterized by the formation and decay of metastable $pp\pi$ molecules) is expected to lead to the following new features of the cascade.

(1) The decay through the intramolecular absorption gives a continuous distribution of pionic atoms in the energy range 0–60 eV, in contradistinction to the discrete distribution originating from the direct Coulomb deexcitation. This process (at room temperature, 0.04 eV) is some ten times faster than the direct Coulomb deexcitation, and although it in most cases results in low energy (0–10 eV) pionic atoms, it has a considerable effect on the cascade in that it influences the disappearance rate of excited $p\pi$ atoms out of the initial (entrance) channel.

(2) The Coulomb decay results in a cluster of energies confined to the interval 0–2 eV below the characteristic energy of direct Coulomb deexcitation. This process, however, needs to compete with a (faster) Auger process [see (3) below].

(3) The decay via the Auger channel gives again a (less excited) $pp\pi$ state, and therefore ends up with intramolecular decay described in (1) above, or in a series of discrete energies of pionic atoms according to (2). In the latter case the discrete energies are shifted downwards with respect to the characteristic energy of direct Coulomb deexcitation by 7–50 eV [the exact energies are given by Eq. (11), with binding energies given in Table V]. The rate of this process is comparable to the rate for direct Coulomb $n_i=3\rightarrow n_f=2$ deexcitation (see Fig. 5). For higher n's the direct transition rate increases rapidly. Therefore the resonant process should become progressively less important for more highly excited pionic atoms. For the transition $n_i=2\rightarrow n_f=1$ the resonant process would dominate over the direct process, but in this case nuclear absorption will totally dominate over all other processes. It should be noted that our approach delivers the *total* widths for the Coulomb decay, meaning that we automatically incorporate the possibility of decays with $\Delta n=n_i-n_f>1$ according to Eq. (46).

In the discussion above we have compared these new acceleration processes to the direct process, which so far has alone been considered responsible for the reacceleration of pionic atoms. The most recent calculation of this rate was made by Ponomarev and Solovev [28]. Their result for the nonresonant transition $n_i=3\rightarrow n_f=2$ at collisional energy corresponding to room temperature (0.04 eV) is 3.1×10^{10} s^{-1}, i.e., of the same order of magnitude as the resonant Auger process estimated above. The cascade of pionic hydrogen atoms has been simulated using Monte Carlo methods [5,6]. To obtain agreement with experimental findings a scaling of the theoretical rate for the direct Coulomb deexcitation (taken from an older calculation by Bracci and Fiorentini [29] which yielded much higher rates than those in [28]) had to be introduced. For the $n_i=3\rightarrow n_f=2$ transition at 0.04 eV the optimum rate for direct Coulomb deexcitation would then be about 3×10^{11} s^{-1}. It is our hope that the inclusion of the three effects mentioned above, together with improved calculations of the direct Coulomb deexcitation such as those in [28], in Monte Carlo simulations will improve the agreement with experimental results without any scalings.

VIII. CONCLUSIONS

We have shown that there exists a number of metastable molecular $pp\pi$ states located just below the $p\pi(n=2,3)+p$ thresholds, and proposed that these states can be formed in $p\pi$-H_2 collisions. Our estimates of the relevant rates show that the formation of such states can play an important role for the acceleration of excited pionic hydrogen atoms undergoing cascade in molecular hydrogen. Two different acceleration mechanisms are important, the Coulomb decay, with or without an intermediate Auger decay, of a $pp\pi$ state, giving a discrete kinetic energy to the $p\pi$ atom, and the intramolecular absorption from a $pp\pi$ state, giving a continuous distribution of apparent kinetic energy. To improve the assessment of the importance of these mechanisms one has to (a) improve our estimate of the different partial formation rates, particularly, include the effects on the $pp\pi$ molecule from the surroundings, (b) take into account the combined effect of many resonances, possibly include interferences between them, and (c) improve the estimate of the competing acceleration via direct Coulomb deexcitation.

ACKNOWLEDGMENTS

This work was supported by the National Science Foundation through a grant for the Institute for Theoretical Atomic and Molecular Physics (ITAMP) at Harvard University and Smithsonian Astrophysical Observatory, and by the Swedish Natural Science Research Council (NFR). The computations were supported by the Swedish Council for High Performance Computing (HPDR) and Parallelldatorcentrum (PDC) at the Royal Institute of Technology, the TRACS Program of the European Commission, and Kyushu University, Japan. We wish to express our gratitude to M. Kamimura, E. C. Aschenauer, and the staff of ITAMP for fruitful discussions. We also thank H. Karlsson for useful information regarding the Lanczos and Arnoldi methods.

[1] J. F. Crawford *et al.*, Phys. Rev. D **43**, 46 (1991).
[2] W. K. McFarlane *et al.*, Phys. Rev. D **32**, 547 (1985).
[3] J. F. Crawford *et al.*, Phys. Rev. Lett. **56**, 1043 (1986).
[4] J. F. Crawford *et al.*, Phys. Lett. B **213**, 391 (1988).
[5] E. C. Aschenauer and V. E. Markushin, Hyperfine Interact. **101/102**, 97 (1996).
[6] E. C. Aschenauer *et al.*, Phys. Rev. A **51**, 1965 (1995).
[7] A. Badertscher *et al.*, Phys. Lett. B **392**, 278 (1997).
[8] P. Froelich and A. Flores-Riveros, Phys. Rev. Lett. **70**, 1595 (1993).
[9] P. Froelich and J. Wallenius, Phys. Rev. Lett. **75**, 2108 (1995).
[10] J. Wallenius and P. Froelich, Phys. Rev. A **54**, 1171 (1996).
[11] J. Wallenius and P. Froelich, Phys. Lett. A **206**, 73 (1995).
[12] E. Vesman, Pis'ma Zh. Éksp. Teor. Fiz. **5**, 113 (1967) [JETP Lett. **5**, 91 (1967)].
[13] M. Kamimura, Phys. Rev. A **38**, 621 (1988).
[14] D. R. Bates and R. H. G. Reid, Adv. At. Mol. Phys. **4**, 13 (1968).
[15] R. J. LeRoy, University of Waterloo, Ontario, Canada Chem. Phys. Res. Report No. CP-555, 1995.
[16] W. Kołos, Adv. Quantum Chem. **5**, 99 (1970).
[17] S. T. Epstien, J. Chem. Phys. **44**, 836 (1966).
[18] V. I. Korobov, Hyperfine Interact. **101/102**, 307 (1996).
[19] C. J. Joachain, *Quantum Collision Theory* (North-Holland Publishing Company, Amsterdam, 1975), Chap. 20.
[20] T. Ericson and W. Weise, *Pions and Nuclei* (Oxford University Press, Oxford, 1988), Chap. 6.3.
[21] W. Beer *et al.*, Phys. Lett. B **261**, 16 (1991).
[22] J. Wallenius and M. Kamimura, Hyperfine Interact. **101/102**, 319 (1996).
[23] W. P. Reinhardt, Annu. Rev. Phys. Chem. **33**, 223 (1982).

[24] G. H. Golub and C. F. Van Loan, *Matrix Computations* (The Johns Hopkins University Press, Baltimore, 1989).
[25] D. J. Schneider and J. H. Freed, Adv. Chem. Phys. **LXXIII**, 387 (1989).
[26] Y. Kino and M. Kamimura, Hyperfine Interact. **101/102**, 191 (1996).
[27] R. Frosch, Paul Scherrer Institute Internal Report No. TM-37-21, 1985 (unpublished).
[28] L. I. Ponomarev and E. A. Solovev, Pis'ma Zh. Éksp. Teor. Fiz. **64**, 129 (1996) [JETP Lett. **64**, 135 (1996)].
[29] L. Bracci and G. Fiorentini, Nuovo Cimento A **43**, 9 (1978).